Article

Not peer-reviewed version

Synthesis and Characterization of Tetraphenylethene AIEgen-Based Push-Pull Chromophores for Photothermal Applications: Do the Cycloaddition – Retroelectrocyclization Click Reaction Could Make any Molecule Photothermally Active?

Maxime Roger , Yann Bretonnière , Yann Trolez , Antoine Vacher , Imane Arbouch , Jérôme Cornil , Gautier Félix , Julien De Winter , Sébastien Richeter , Sébastien Clément * , Philippe Gerbier *

Posted Date: 17 April 2023

doi: 10.20944/preprints202304.0393.v1

Keywords: TPE; AIEgen; cycloaddition-retroelectrocyclization; CA-RE; click chemistry; photothermal applications

Article

Synthesis and Characterization of Tetraphenylethene Aiegen-Based Push-Pull Chromophores for Photothermal Applications: Do the Cycloaddition—Retroelectrocyclization Click Reaction Could Make Any Molecule Photothermally Active?

Maxime Roger [1], Yann Bretonnière [2], Yann Trolez [3], Antoine Vacher [3], Imane Arbouch [4], Jérôme Cornil [4], Gautier Félix [1], Julien De Winter [5], Sébastien Richeter [1], Sébastien Clément [1,*] and Philippe Gerbier [1,*]

[1] Univ. Montpellier, ICGM, UMR 5253, CNRS, ENSCM, 34293 Montpellier, France.
[2] Univ. Lyon 1, ENSL, CNRS, UCBL, Laboratoire de Chimie UMR 5182, 69364 Lyon, France.
[3] Univ Rennes, Ecole Nationale Supérieure de Chimie de Rennes, CNRS, ISCR - UMR 6226, F-35000 Rennes, France.
[4] Univ. Mons-UMONS, Laboratory for Chemistry of Novel Materials, 7000 Mons, Belgium.
[5] Univ. Mons-UMONS, Organic Synthesis and Mass Spectrometry Laboratory (S2MOs), 7000 Mons, Belgium.
* Correspondence: SC: sebastien.clement1@umontpellier.fr; PG: philippe.gerbier@umontpellier.fr

Abstract: Three new tetraphenylethene (TPE) push-pull chromophores exhibiting strong intramolecular charge transfer (ICT) are described. They were obtained via [2+2] cycloaddition - retroelectrocyclization (CA-RE) click reactions on an electron-rich alkyne-tetrafunctionalized TPE (TPE-alkyne) using both 1,1,2,2-tetracyanoethene (TCNE), 7,7,8,8-tetracyanoquinodimethane (TCNQ) and 2,3,5,6-tetrafluoro-7,7,8,8-tetracyanoquinodimethane (F_4-TCNQ) as electron-deficient alkene. Only the starting **TPE-alkyne** displayed a significant AIE behavior, whereas for **TPE-TCNE**,a faint effect was observed and for **TPE-TCNQ** and **TPE-F_4-TCNQ**, no fluorescence was observed in any conditions. The main ICT bands that dominate the UV-Visible absorption spectra underwent a pronounced red-shift beyond the near-infrared (NIR) region for **TPE-F_4-TCNQ**. Based on TD-DFT calculations, it was shown that the ICT character shown by the compounds exclusively originated from the clicked moieties independently of the nature of the central molecular platform. Photothermal (PT) studies conducted on both **TPE-TCNQ** and **TPE-F4-TCNQ** in the solid state revealed excellent properties, especially for **TPE-F4-TCNQ**. These results indicated that CA-RE reaction of TCNQ or F_4-TCNQ with donor-substituted are promising candidates for PT applications.

Keywords: TPE; AIEgen; cycloaddition-retroelectrocyclization; CA-RE; click chemistry; photothermal applications

1. Introduction

Although the phenomenon has been known and briefly described before [1], it is up to Ben Zhong Tang to have first described and tried to explain the unusual behavior of the 1-methyl-1,2,3,4,5-pentaphenylsilole, which was not luminescent in solution in a good solvent but became highly emissive in the solid state [2]. This very rare behavior, called Aggregation Induced Emission (AIE), is opposed to the behavior classically encountered in fluorophores with a planar and rigid structure, which are generally fluorescent in solution and non-emissive in the solid state (Aggregation-Caused Quenching - ACQ). Following this work, in just over 20 years, the number of publications concerning the description of new AIE luminogens (AIEgens) has increased exponentially [3] and the knowledge of the mechanisms leading to the observation of this

phenomenon are now well known [4–6]. The considerable success of the AIE phenomenon lies in the fact that it makes possible it to address effectively to a major issue which is the emission in the solid or aggregated state of molecules, a problem of the utmost importance for many scientific fields or technological applications [4,7,8]. Among the many areas taking advantage of AIEgens, we can mention optoelectronics with OLEDs [9,10], stimuli-responsive materials [11–13], anticounterfeiting or encryption [12,14], sensing [15–17], and biology or medicine, fields in which the use of AIEgens has enabled spectacular advances [18–23]. Indeed, AIEs are used in the fields of imaging [24,25], elucidation of biological processes [26–28], innovative therapies such as photodynamic therapy (PDT) [29–31], photothermal therapy (PTT) [32,33], sonodynamic therapy enhancement [34], cocktail therapy [35] and theranostics [36,37]. Due to the specificity of biological applications, it is necessary to trigger the AIEgens with light in the near-infrared (NIR) domain which has the advantage on the one hand of not being harmful to the cells and on the other hand of having a good depth of penetration into the living tissues [38,39]. As a result, it was necessary to substantially reduce the HOMO-LUMO energy gap (E_g) of conventional AIEgens whose absorption bands are located rather in the UV range. Different strategies can be considered to increase the excitation and emission wavelengths of the fluorophores. The first one consists in increasing the conjugation length of the π-system. However, this strategy is rapidly depleted due to solubility issues, which require "decorating" the molecules with flexible chains. The second one consists in introducing electron attracting (A) and/or donating (D) groups into the π-conjugated system [40–42]. Such groups induce changes in orbital energy levels, either an increase in HOMO energy level (influence of donor group), or a decrease in LUMO energy level (influence of attracting group) of the molecule leading to a narrowing of the E_g [43]. Among the attractor groups yielding the best results are the dicyanovinyl groups. For instance, the latter can be introduced via a Knoevenagel condensation reaction of malonitrile on an AIEgen functionalized with a carbonyl [39,44]. Another approach consists in taking advantage of the "click-chemistry" introduced by K. B. Sharpless because it is effective in introducing various groups under mild, catalyst-free and atom-saving conditions.[45] More especially, the [2 + 2] cycloaddition-retroelectrocyclizations (CA-RE) that involve the reaction between an electron-rich alkyne and an electron-deficient alkene (Scheme 1) have recently attracted significant attention [46,47]. The CA-RE reaction was first reported by M. I. Bruce in 1981 in the field of organometallic chemistry by reacting 1,1,2,2-tetracyanoethene (TCNE) with metallocene-substituted acetylides [48]. It was 18 years later that it was used for the synthesis of DA-type thiophenevinylidene derivatives for nonlinear optical (NLO) applications in the groups of A. K.-Y. Jen and U. W. Suter [49,50]. This reaction has been widely exploited and studied in the group of F. Diederich to develop a new platform of simple molecules with nonlinear optical (NLO) properties [51,52]. In the continuation of these works, he showed that it was possible to modulate the optical and electrochemical properties of the clicked compounds by extending the CA-RE reaction to other electron-deficient alkene which have a similar reactivity such as 7,7,8,8-tetracyanoquinodimethane (TCNQ) and 2,3,5,6-tetrafluoro-7,7,8,8-tetracyanoquinodimethane (F_4-TCNQ) [53–55]. Since then, researchers have used CA-RE to synthesize D-π-A push-pull systems to be used in various applications such as optoelectronics [56–68], NLO [69–71], photoacoustic (PA) imaging [72–76] and theranostics [77]. Surprisingly, although the photoacoustic and photothermal (PT) phenomena are related, very few papers describes the use of CA-RE clicked products for PT applications [72,78].

In this work, we used the [2 + 2] CA-RE reaction with the aim of obtaining new AIE-based PT materials displaying a strong charge transfer character. We chose the AIEgen archetypal tetraphenylethene (TPE) as the central core due to its very good ability to retain its AIE properties although it is incorporated in more complicated molecular architectures [79,80]. Moreover, when linked to naphthalene diimide-fused 2-(1,3-dithiol-2-ylidene)acetonitriles derivatives, it has already shown its ability to lead to AIE-based PT materials.[81] In order to achieve the CA-RE reactions, we have functionalized the four arms of the TPE with C≡C triple bonds capped by dialkylanilino moieties as electron-donor groups. The resulting clicked products with TCNE, TCNQ and F_4-TCNQ showed a pronounced CT characterized by a NIR strong absorption, with in particular, for **TPE-TCNQ** and **TPE-F_4-TCNQ**, in the biological transparency window (NIR-I, 750-1000 nm). These two latter

Preprints (www.preprints.org) | NOT PEER-REVIEWED | Posted: 17 April 2023 doi:10.20944/preprints202304.0393.v1

products were found to possess good thermal properties allowing them to display rather good photothermal performances.

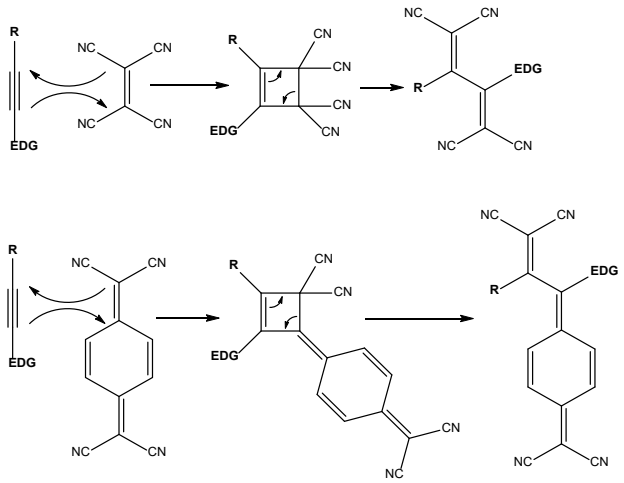

Scheme 1. Mechanism of the CA-RE click-reaction between TCNE (top) or TCNQ (bottom) and alkynes activated by an electron-donor group (EDG). When TCNQ is used, the quinoidal moiety is located next to the EDG group [54,82].

2. Results and discussion

2.1. Synthesis

The preparation of compounds **TPE-TCNE**, **TPE-TCNQ** and **TPE-F$_4$-TCNQ** started from **TPE-alkyne** whose synthesis involved a McMurry homocoupling reaction of the benzophenone derivative **Bz-alkyne** with a yield of 55% (Scheme 2). **Bz-alkyne** was synthesized in 71% yield by using a Sonogashira cross-coupling reaction between 4,4′-dibromobenzophenone and N,N′-didodecyl-4-ethynylaniline. All attempts to obtain **TPE-alkyne** through a Sonogashira cross-coupling reaction between 1,1,2,2-tetrakis(4-bromophenyl)ethene and N,N′-didodecyl-4-ethynylaniline invariably conducted to inseparable mixtures of diversely substituted compounds.

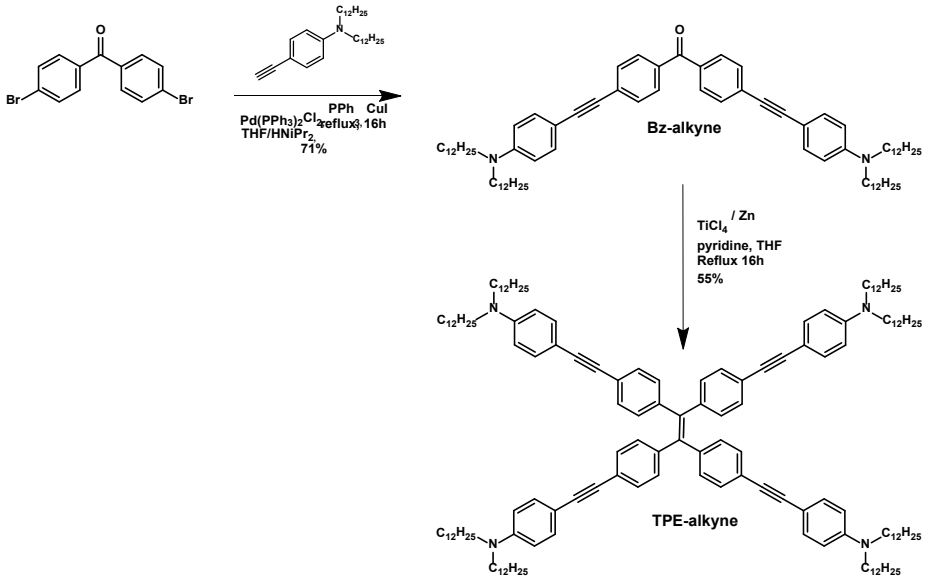

Scheme 2. Reaction pathway towards **TPE-alkyne**.

Finally, [2+2] CA-RE reactions were conducted by using a 50% excess of tetracyano derivatives (TCNE, TCNQ and F4-TCNQ) in various solvents at room temperature to afford **TPE-TCNE**, **TPE-**

Preprints (www.preprints.org) | NOT PEER-REVIEWED | Posted: 17 April 2023 doi:10.20944/preprints202304.0393.v1

TCNQ and **TPE-F4-TCNQ** respectively, as dark film-forming solids after purification by column chromatography on silica gel (Scheme 3).

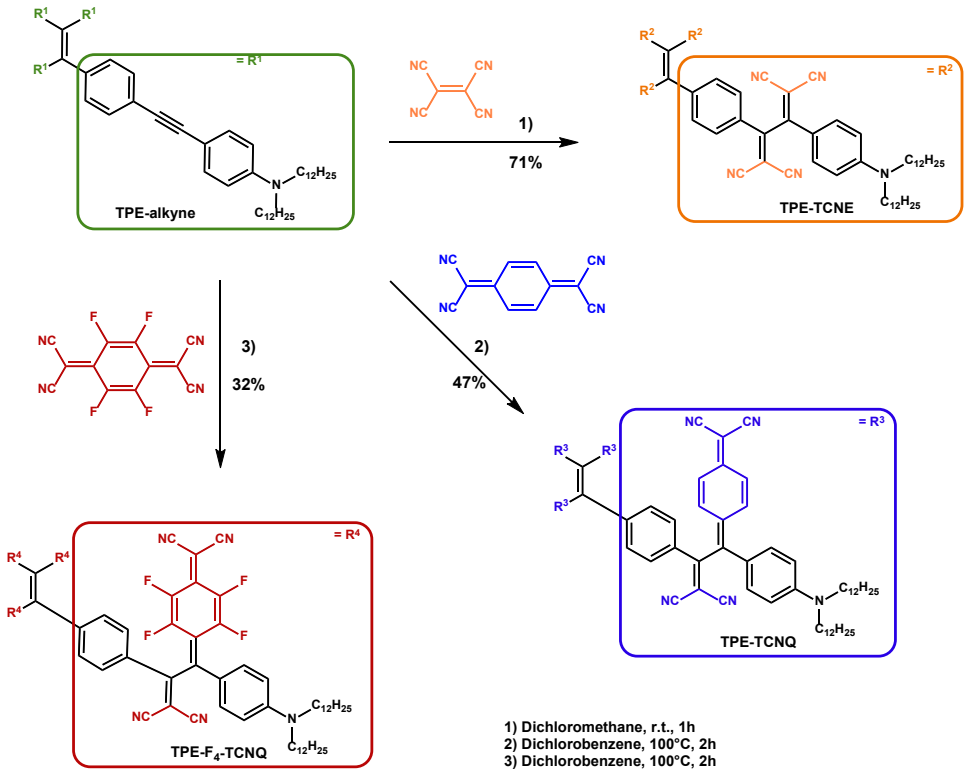

Scheme 3. Synthetic scheme of compounds TPE-alkyne, TPE-TCNQ and TPE-F4-TCNQ.

All the compounds were fully characterized by ^{1}H, $^{13}C\{^{1}H\}$, $^{19}F\{^{1}H\}$ NMR spectroscopy and high-resolution mass spectrometry (HR-MS) (see ESI for spectral details). Examining their ^{1}H NMR spectra, some interesting points can be noted (Figure 1): *i*) as expected, the grafting of electron withdrawing groups on the triple bond led to a deshielding of the protons located in their vicinity (doublets in the aromatic region) as well as those of the methylene groups bonded to the nitrogen atoms of the aniline moieties (δ = 3.25 – 3.55 ppm); *ii*) the comparison of the chemical shifts of the aromatic protons between **TPE-alkyne**, **TPE-TCNE** and **TPE-TCNQ** highlighted the localization of dicyanoquinomethanyl moiety on the aniline side in agreement with previous findings [54]; *iii*) due to the highly twisted conformation of the butadiene in **TPE-TCNQ** (see ESI), all the protons present in the quinoid ring are not equivalents giving rise to four doublets among which two are clearly seen in the figure (see ESI for more details) and *iv*) the spectrum obtained for **TPE-F4-TCNQ**, is poorly resolved witnessing the presence of paramagnetic species as observed elsewhere.[46,53] Indeed, the ESR spectrum of a THF solution of **TPE-F4-TCNQ** showed an unresolved weak signal with a *g* factor of 2.0027 and a band width of 7.50 G, whereas in the solid state, a much more intense signal with *g* factor of 2.0021 and a band width of 10.25 G is observed (Figure 2).

Preprints (www.preprints.org) | NOT PEER-REVIEWED | Posted: 17 April 2023 doi:10.20944/preprints202304.0393.v1

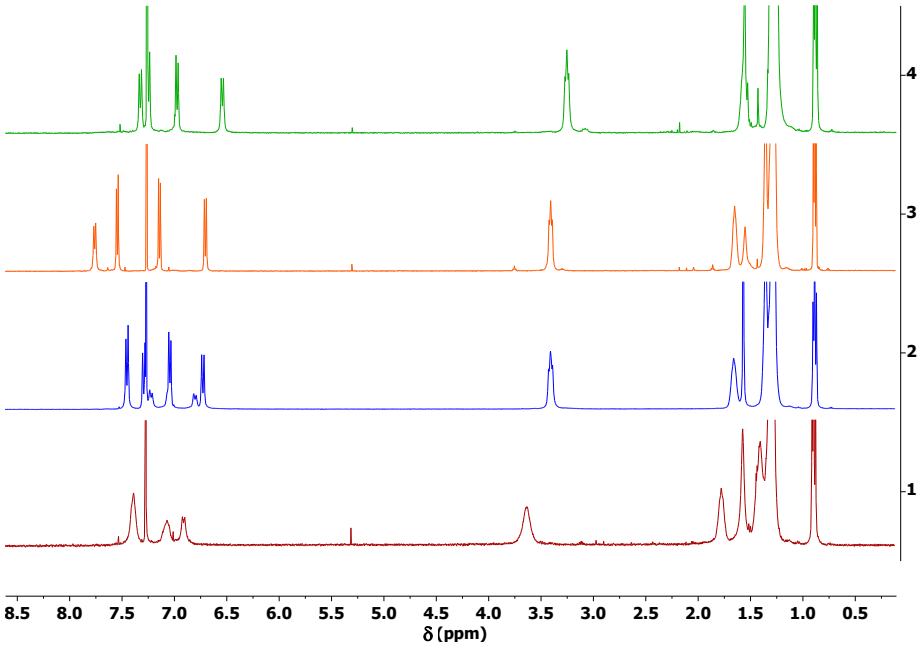

Figure 1. ^{1}H NMR spectra of **TPE-alkyne** (green), **TPE-TCNE** (orange), **TPE-TCNQ** (blue) and **TPE-F$_4$-TCNQ** (red) recorded in $CDCl_3$.

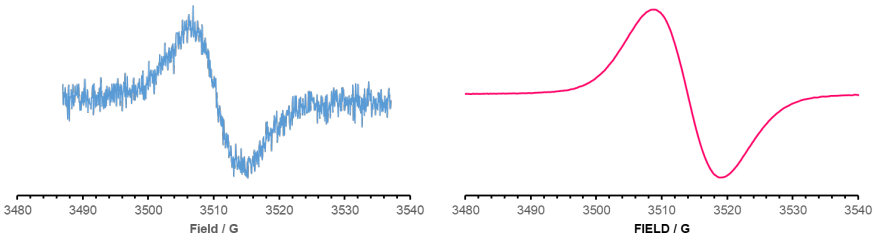

Figure 2. ESR spectra of **TPE-F$_4$-TCNQ** in THF solution (right) and in the solid state (left) recorded at room temperature.

2.2. Photophysical properties

The UV-Visible absorption spectra of the investigated compounds are shown in Figure 3. The starting compound TPE-alkyne only showed a major absorption peak at 359 nm corresponding to a π-π* transition (*vide supra*). Contrastingly, the spectra of **TPE-TCNE**, **TPE-TCNQ** and **TPE-F$_4$-TCNQ** showed additional intense absorption peaks in the visible-NIR region (see Table 1 for data). These peaks possessed strong molar extinction coefficients likely corresponded to intramolecular charge transfer (ICT) absorptions involving the terminal amino groups and dicyanovinylic moieties [76]. Moreover, as observed previously, the effect of the increasing electron-withdrawing strength of the adduct that is F$_4$-TCNQ > TCNQ > TCNE is witnessed by a marked bathochromic shift of the CT absorption [70–72,83–86]. Besides the intense charge transfer band involving the dicyanoquinoïd moieties (CT band B) observed above 600 nm for **TPE-TCNQ** and **TPE-F$_4$-TCNQ** , the less intense CT band (CT band A) that was observed for all the clicked compounds in the 450-550 nm region involved the dicyanovinylic moieties (see Figure 4) [76]. Finally, although this is commonly observed for compounds exhibiting a charge transfer phenomenon, we have not demonstrated solvatochromism for these TPE-adducts [66]. This may be related to the symmetry of these molecules, which implies that they have a weak total dipolar moment in the excited state. The absorbance spectra of all adducts deposited as thin films on quartz slides were like those recorded in THF solutions (Figure S23). As

Preprints (www.preprints.org) | NOT PEER-REVIEWED | Posted: 17 April 2023 doi:10.20944/preprints202304.0393.v1

seen in Table 1, the longer wavelength absorptions experienced moderate (TPE-TCNE: 7 nm and TPE-4F-TCNQ: 15 nm) to appreciable (TPE-TCNQ: 50 nm) red-shifts in the solid state.

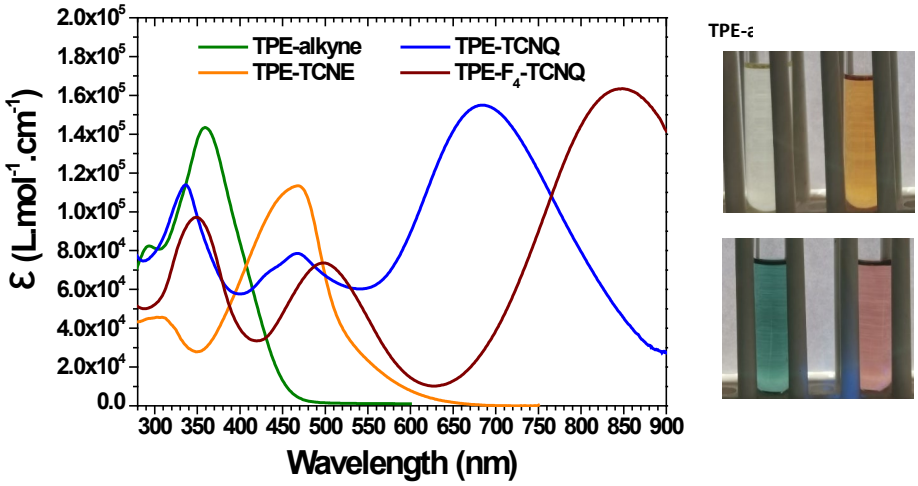

Figure 3. UV-Visible absorption spectra of investigated compounds in THF solutions (C = 6.10^{-6} M) (left) and images of their corresponding solutions (right).

Table 1. Optical data (absorbance and fluorescence) for the investigated compounds recorded in solution or in the aggregated state.

	TPE-alkyne	TPE-TCNE	TPE-TCNQ	TPE-F4-TCNQ
Absorbance in solution[a] *(nm) /(ε (L.mol^{-1}.cm^{-1}))*	294 (82 400) 359 (143 400)	307 / (45 600) 469 (113 400)	337 (113 900) 468 (78 500) 688 (155 000)	348 (97 500) 497 (73 600) 849 (163 400)
Absorbance as thin films (nm)	-	476	471, 738	498, 864
$\lambda_{em\ max}$ *(solution*[a] */ aggregated*[b]*)*	582 / 560 / -	≈700 / 786	-	-
Φ_{sol} *(%)*[a]	13%	-	-	-
Φ_{aggr} *(%)*[b]	21%	NM	-	-
λ_{onset} *(nm)*[c]	460	540	900	-
$E_{g\ opt}$ *(eV)*[d]	2.70	2.30	1.38	-

[a] measured in THF, [b] 10% THF / 90% H_2O, [c] Estimated from the extrapolation of the absorption curve of **TPE-TCNQ**, [d] Calculated using the relation E = $1.6.10^{-19}$ (h.c/λ_{onset}). NM: not measurable.

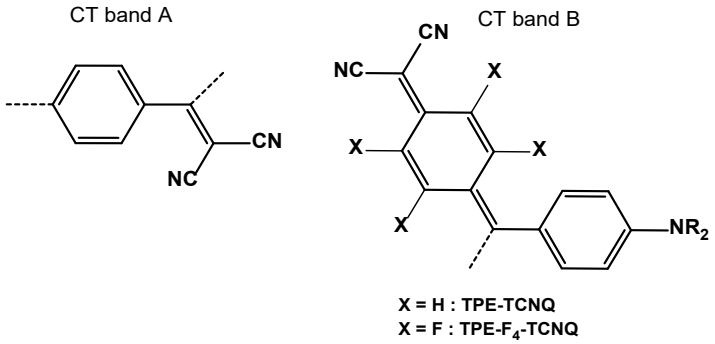

Figure 4. Chromophores likely involved in the CT bands A and B.

The fluorescence spectra were also recorded both in solution (THF) and in the aggregated state for all compounds. As observed in most cases with CA-RE products [87–89], only **TPE-alkyne**

Preprints (www.preprints.org) | NOT PEER-REVIEWED | Posted: 17 April 2023 doi:10.20944/preprints202304.0393.v1

precursor and **TPE-TCNE** exhibited measurable fluorescence with an emission maximum at 582 nm. The corresponding spectra are shown in Figure 5. Interestingly, the emission maximum showed a dependence on the pH of the solution with a red-shift of 44 nm in acidic medium (see Figure S26). As observed with most TPE derivatives, the emission intensity increased markedly when going from the solution to the aggregated state, indicating an AIE behavior [79]. Consequently, we decided to follow the evolution of the emission spectra of both **TPE-alkyne** and **TPE-TCNE** in various mixtures of THF/water, water being a bad solvent for these compounds that should induce an aggregation phenomenon from a certain percentage. As shown in Figure 6, the emission intensity gradually increased as the water percentage exceeded 20% for **TPE-alkyne** and more abruptly above 70% for **TPE-TCNE**, indicating that the presence of the dicyanovinylic moieties induced an increase in water solubility. Interestingly, both compounds exhibited an opposite shift when passing from the solvated to the aggregated state, **TPE-alkyne** experiencing a slight blue-shift whereas for **TPE-TCNE,** a more pronounced red-shift is noticed.

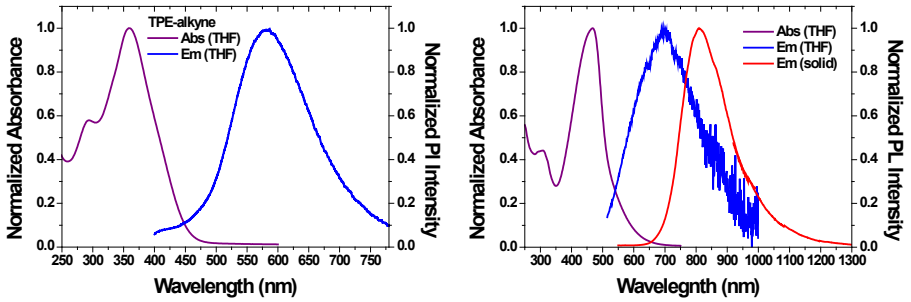

Figure 5. UV-Visible absorption and fluorescence spectra of **TPE-alkyne** (A) and **TPE-TCNE** (B) recorded in solution and in the solid state.

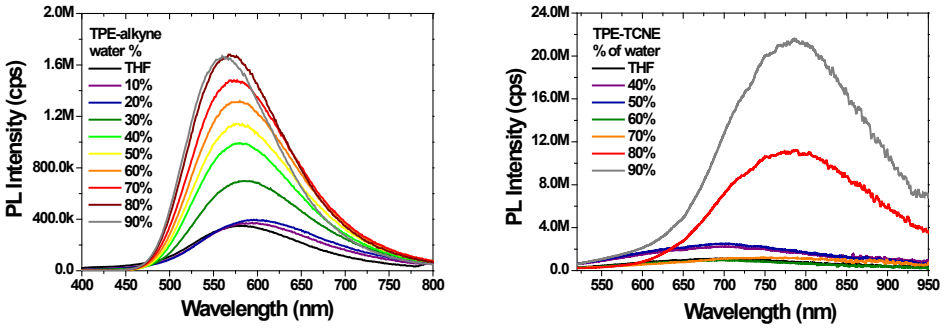

Figure 1. Evolution of the emission spectra as a function of water content in THF solutions for **TPE-alkyne** (left) and **TPE-TCNE** (right).

2.3. Electrochemistry

To evaluate the electronic properties of the different cycloadducts, their cyclic voltammograms (CVs) were recorded as well as the CV of the **TPE-alkyne** precursor for comparison (see Figure 7). This latter only shows one irreversible oxidation wave around 0.80 V *vs.* SCE (peak potential), which could be attributed to the oxidation of the four anilines. One can notice that the four oxidations occur at the same potential, probably because of the low conjugation between anilines due to the twisted geometry around the central TPE core. This irreversible oxidation was also observed in the case of cycloadducts but it is shifted to higher potentials (peak potentials at 1.31 V *vs.* SCE for **TPE-TCNE**, 0.88 V *vs.* SCE for **TPE-TCNQ** and 0.97 V *vs.* SCE for **TPE-F$_4$-TCNQ**). This may be attributed to the presence of the strong electron-acceptors conjugated to the anilines rendering their oxidations more difficult. By contrast with the **TPE-alkyne** precursor, two reversible reduction waves were also observed. The reduction potentials strongly depend on the nature of the electron-accepting groups. In the case of **TPE-TCNE**, the two reductions occur at -0.45 and -0.88 V *vs* SCE, which are in line with

Preprints (www.preprints.org) | NOT PEER-REVIEWED | Posted: 17 April 2023 doi:10.20944/preprints202304.0393.v1

previously reported values for this kind of tetracyanobutadienes (TCBD).[52] **TPE-TCNQ** is easier to reduce with reductions at -0.23 and -0.46 V *vs.* SCE due toa higher delocalization of the newly formed negative charges thanks to the dicyanoquinodimethane moiety. The reductions potentials are even higher in the case of **TPE-F$_4$-TCNQ**: +0.09 and -0.21 V *vs.* SCE due to the significant strengthening of the electron-accepting ability of dicyanoquinodimethane moiety due to the presence of the fluorine atoms.[54] This particularly high first reduction potential may explain the "spontaneous" reduction of the system that generates the above-mentioned ESR signal in solution and in the solid state.

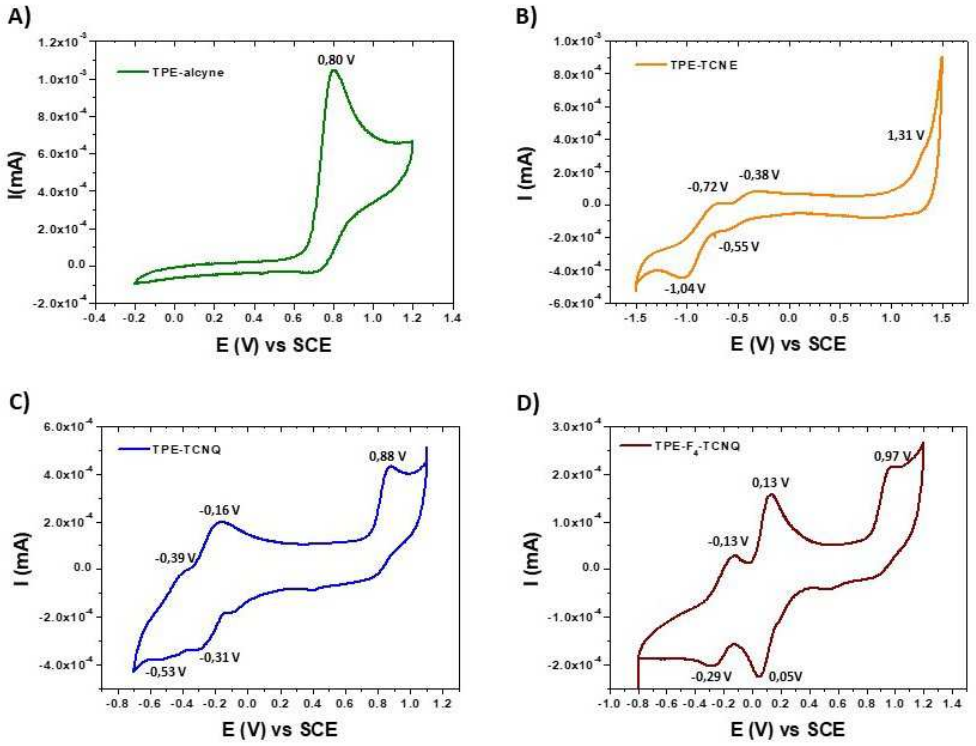

Figure 7. Cyclic voltammograms of **TPE-alkyne** (A), **TPE-TCNE** (B), **TPE-TCNQ** (C) and **TPE-F$_4$-TCNQ** in CH_2Cl_2 + Bu_4NPF_6 solutions. Scan rate: 100 mV.s^{-1}, Pt disk working electrode. Potentials are given *vs.* SCE.

Table 2. Electrochemical data extracted from cyclic voltammetry in dichloromethane with 0.2 M of NBu_4PF_6 as electrolyte (potentials versus saturate calomel electrode).

	TPE-alcyne	TPE-TCNE	TPE-TCNQ	TPE-F$_4$-TCNQ
$E_{1/2}$ (V) [a]	-	-0.45	-0.23	+0.09
		-0.88	-0.46	-0.21
E_p [b]	+0.80	+1.31	+0.88	+0.97

[a] $E_{1/2} = (E_{pc} + E_{pa})/2$, in which E_{pc} and E_{pa} correspond to the cathodic and anodic peak, respectively (this potential is calculated when the electron transfer is reversible) [b] E_p = potential peak (irreversible wave).

2.4. Electronic structure calculations

To gain more insights into the photophysical and electrochemical measurements on the four TPE derivatives, theoretical calculations based on (Time-Dependent) Density Functional Theory (TD)-DFT have been performed [90–94]. All calculations have been carried out using the long-range hybrid CAM-B3LYP functional [95] and a 6-311G (d,p) basis set, as motivated by the fact that the DFT functionals with long-range corrections better describe excited states with a pronounced charge transfer character [96].

The shape of the frontier orbitals in the optimized structures obtained from the DFT calculations are displayed in Figure 8 (see also Figure S44). For **TPE-alkyne**, the HOMO is delocalized evenly on the entire molecule while the **LUMO** is denser on the TPE core. In **TPE-TCNE**, the HOMO is localized

Preprints (www.preprints.org) | NOT PEER-REVIEWED | Posted: 17 April 2023 doi:10.20944/preprints202304.0393.v1

on the extremity of one TCBD arm following the introduction of an electron-accepting group in its center, thus breaking apart the large delocalization observed for the pristine compound. Similarly, the HOMO-1 to HOMO-3 levels get localized over the other branches (Figure S46). The LUMO spreads along a diagonal involving both the TPE core and the inner part of two TCBD arms. A similar pattern prevails for the LUMO+1 while the LUMO+2 and LUMO+3 are delocalized over the other diagonal (Figure S46). In the case of **TPE-TCNQ** and **TPE-F$_4$-TCNQ**, the frontier orbital spatial distribution is quite similar, with the HOMO and LUMO levels localized over the terminal donor part and inner acceptor part, respectively, of a single arm. The deeper occupied and higher unoccupied levels are localized over the other branches. Here, the TPE core is thus weakly involved in the frontier orbital distribution. Excited states with a pronounced intra- and/or interbranch character are thus expected at low energy. Noteworthy, since the molecular orbitals are not uniformly distributed over all branches, these frontier molecular orbitals are quasi-degenerate, particularly the HOMOs (see Figures S45 and S46).

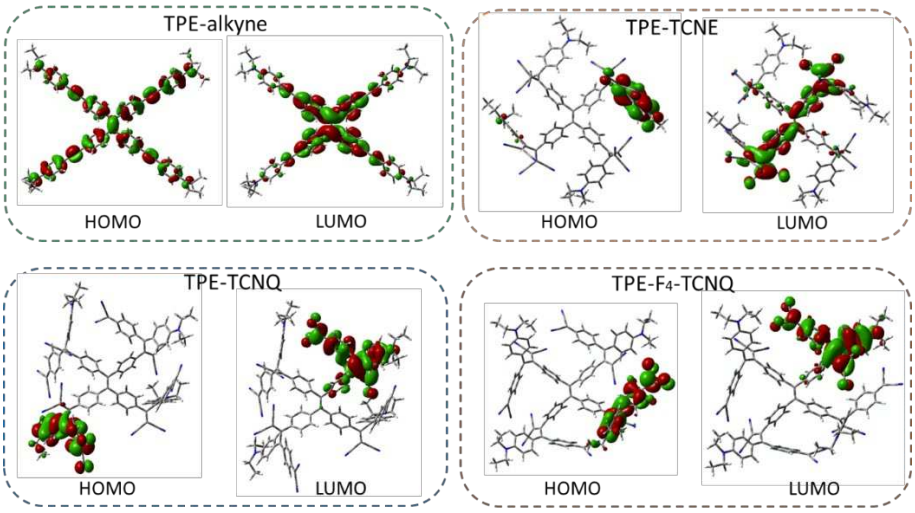

Figure 8. Frontier orbitals of the investigated compounds from the CAM-B3LYP/6.311g(d,p)-calculated optimized structures. Isovalues are set to 0.02 e/au^3.

The relative energy level alignment of the frontier orbitals of the TPE-adducts has been estimated from the DFT calculations and are displayed in Figure 9 when accounting for the solvent effects (*i.e.*, THF used for the optical absorption spectra) via the Polarizable Continuum Model (PCM). As measured in cyclic voltammetry, the calculated HOMO-LUMO gaps decrease when increasing the electron withdrawing character of the adducts, in the following order: F$_4$-TCNQ > TCNQ > TCNE. It is worth remembering that the absolute values of the gap cannot be directly compared to the CV data since the calculations rely on Koopmans' approximation (associating the ionization potential to the HOMO of the neutral molecule and the electron affinity to the LUMO energy). Moreover, the amplitude of the HOMO-LUMO gap critically depends on the choice of the DFT functional. Nevertheless, comparing the evolution of the HOMO and LUMO energies on a relative basis is meaningful. Doing so, we observe that the shift between the frontier energy levels of the various TPE-adducts nicely matches the experimental trends (see Figure 9).

Preprints (www.preprints.org) | NOT PEER-REVIEWED | Posted: 17 April 2023 doi:10.20944/preprints202304.0393.v1

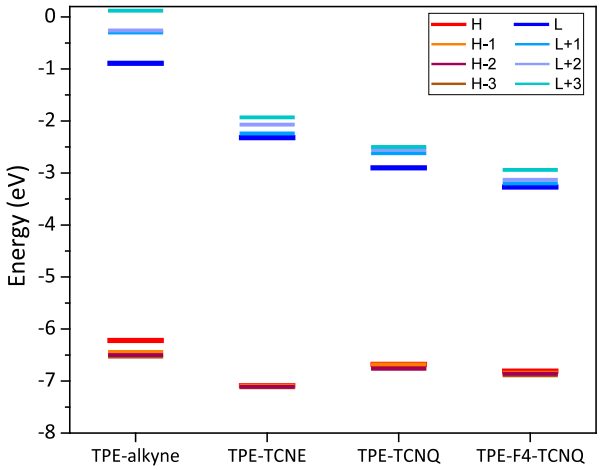

Figure 9. Energy level alignment of the four frontier occupied and virtual molecular orbitals for the investigated systems in THF, as calculated at the CAM-B3LYP/6-311G (d,p) level.

2.5. Excited-state calculations

The absorption spectra of the TPE compounds simulated at the TD-DFT level using the same functional and basis set are shown in Figure 10 (see also Figure S47). The Gaussian broadening used to generate the UV-Visible absorption spectra is set to σ= 0.25 eV to match the width of the experimental bands. The computed electronic transitions as well as their corresponding oscillator strength and assignment are listed in Table S1, SI.

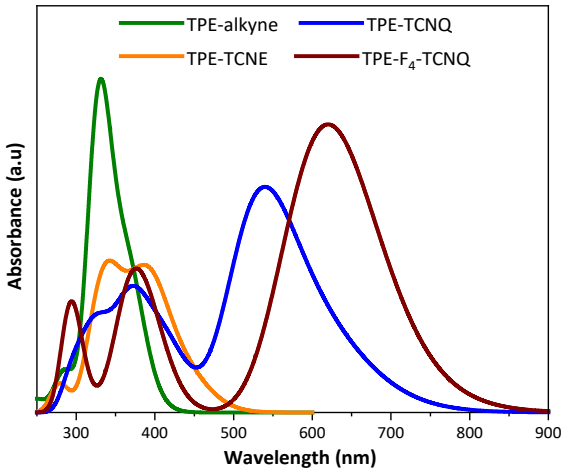

Figure 10. UV-Visible absorption spectra of the investigated compounds in THF simulated at the TD-DFT/CAM-B3LYP level.

For **TPE-alkyne**, the lowest excitation occurs at 367 nm, which is in very good agreement with the strong absorption band experimentally observed in its UV−Visible absorption spectrum (λ_{max} = 359 nm, Table 1, Figure 3). This corresponds to a transition from the HOMO to the LUMO level (see Table S1, SI). Conversely, the absorption spectra of the TPE adducts exhibit an additional absorption band with a CT character in the visible-near infrared region. For **TPE-TCNE**, **TPE-TCNQ** and **TPE-F4-TCNQ**, the lowest excitation occurs at 443 nm, 625 nm and 675 nm, respectively. To further analyze the nature of these excitations, we performed a NTO analysis that describes globally for each given excitation where the electron is excited from and where it is promoted during the excitation, *i.e.*, as a single-particle transition from an effective occupied to virtual orbital [87]. We refer to the occupied and virtual NTOs as "hole" and "electron" transition orbitals, respectively. Note that the NTOs are not the same as the occupied and virtual molecular orbitals calculated in the ground state. Moreover,

Preprints (www.preprints.org) | NOT PEER-REVIEWED | Posted: 17 April 2023 doi:10.20944/preprints202304.0393.v1

we have also calculated the spatial overlap φs between the electron and hole density in order to quantitatively evaluate the charge-transfer character of an electronic transition; φs = 1 for a purely localized character and φs =0 for a pure charge transfer excitation [88,89]. In the case of **TPE-TCNE**, the lowest excitation at 443 nm is predominantly assigned to a transition from a hole orbital localized on the extremity of a TCBD arm to an electron orbital localized on the inner part of the same TCBD arm and including a part of TPE core. This graphical picture of NTOs is consistent with the moderate spatial overlap φs value of 0.47 calculated for this transition (see Figure 11). Moving to **TPE-TCNQ** and **TPE-F4-TCNQ**, the dominant transition contributing to the lowest excitation at 625 nm and 675 nm, exhibits both a weaker charge-transfer character compared to **TPE-TCNE** due to the strong spatial overlap between the hole and electron NTOs orbitals as evidenced by a larger φs index (0.70 and 0.72, respectively) (see Figure 11). For all TPE adducts, the high oscillator strength associated to the lowest excitation is attributed to this strong intra-branch character. Interestingly, the simulated absorption spectra nicely reproduce the experimental bathochromic shift of the CT absorption band. Going from **TPE-TCNE**, **TPE-TCNQ** to **TPE-F4-TCNQ**, a systematic red shift of the CT absorption band as well as an increase of its intensity are noticed, which is fully in line with the increase of the electron withdrawing strength of the TPE adducts and the decrease in the CT character, respectively. This red shift can be evaluated by computing the energy difference between the main peaks of the lowest charge transfer band of the TPE conducts. Thus, moving from **TPE-TCNE** (E_{max}= 3.11 eV) to **TPE-TCNQ** (E_{max} =2.27 eV), a red shift of 0.84 eV is computed whereas a red shift of 0.34 eV is obtained going from **TPE-TCNQ** (E_{max}=2.27 eV) to **TPE-F4-TCNQ** (E_{max} =1.93 eV) (see Figure S46). These results are in excellent agreement with experiments providing the same red shifts of 0.84 eV and 0.34 eV, respectively (see Table 1).

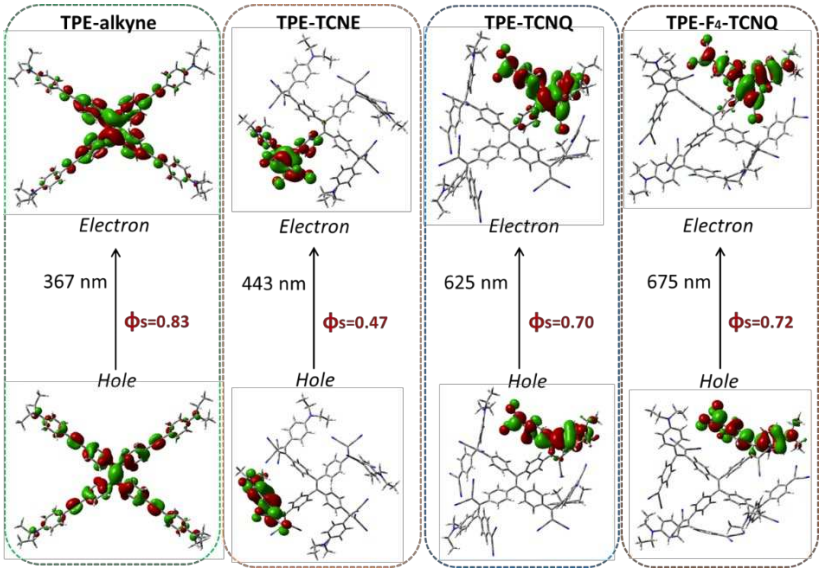

Figure 11. The hole and electron Natural Transition Orbitals (NTOs) for the lowest excitation of the investigated compounds with the associated energy, and φ_s descriptor, computed at the CAM-B3LYP/6-311G(d,p). Isovalues are set to 0.02 e/au^3.

2.6. Photothermal properties and thermal stability

Due to their high absorption in the red-NIR region, **TPE-TCNQ** and **TPE-F4-TCNQ** appear as suitable photothermal agent relaxing to their ground state non-radiatively by creation of phonons (vibrations) and thus, affording a raise of the temperature.[100] To investigate the photothermal behavior of **TPE-TCNQ** and **TPE-F4-TCNQ**, the temperature changes of thin films and powders under a laser beam were measured. Figure S23 shows absorption spectra for **TPE-TCNE**, **TPE-TCNQ** and **TPE-F4-TCNQ** thin films (see ESI for the thin film deposition process). A wavelength of 808 nm was selected for this study for two reasons: (*i*) this wavelengthis in the first biological transparency window (NIR-I, 750-1000 nm), (*ii*) this wavelength is located in a good absorbing region of the UV-

Preprints (www.preprints.org) | NOT PEER-REVIEWED | Posted: 17 April 2023 doi:10.20944/preprints202304.0393.v1

visible absorption spectra of both molecules. In similar conditions, **TPE-F4-TCNQ** shows a stronger photothermal conversion compared to **TPE-TCNQ** (Figure 12). Figure 13 displays photothermal conversion cycles for **TPE-F4-TCNQ** at different laser powers. The thermal cycles are reproducible indicating that the molecules do not degrade under irradiation (see Figure S40). The first cycle was fitted using the COMSOL software to extract the surface heat power produced by the beam light irradiation. In the case of thin films and at the maximum power of the laser (2.58 W/cm^2), the temperature rose to a maximum of 50 °C in less than one minute. If the thin film is replaced by a dense powder of **TPE-F4-TCNQ,** the temperature rose at almost 100 °C in less than one minute (Figure 13). This difference is explained by an increase in the amount of matter of the sample leading to an increase of light absorption in the case of the irradiation of the powder. Finally, to check the thermal stability of **TPE-TCNQ** and **TPE-F4-TCNQ**, a thermogravimetric analysis (TGA) under nitrogen flow was performed indicating no weight loss greater than 2% up to 320 °C (see Figure S36).

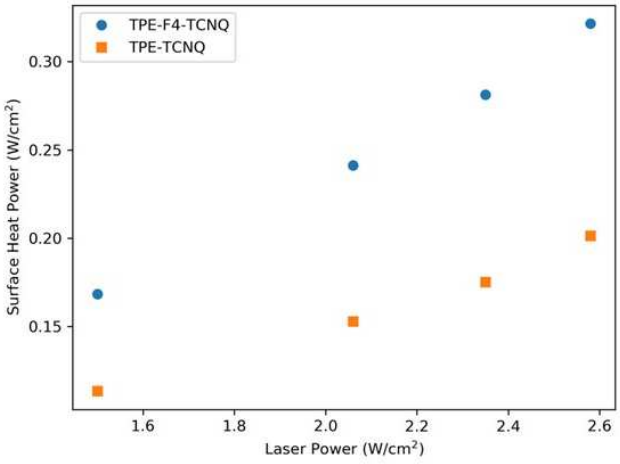

Figure 12. Comparison of the surface heat power *vs.* laser power at 808 nm for **TPE-TCNQ** (orange) and **TPE-F4-TCNQ** as thin films.

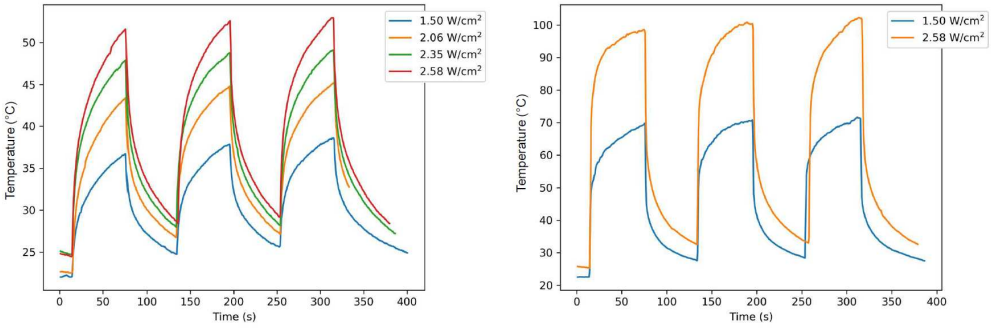

Figure 13. Photothermal conversion behavior of **TPE-F4-TCNQ** under 808 nm laser irradiation at different laser powers (1.50, 2.06, 2.35, and 2.58 cm^{-2}), as a thin film (left) and as a powder (right).

2.7. Concluding remarks

Generally speaking, it is interesting to note that almost all the CA-RE derivatives described in the literature to date have spectral characteristics extremely close to those described in this paper when the electron donating group is a dialkyl or a diphenyl aniline [54,57,59,62,69–74,76,83–86,101–112]. In all cases, the ICT bands are found in the same regions within a few nm. The CT band A is between 450 and 470 nm and the CT band B between 680 and 710 nm for TCNQ and between 830 and 860 nm for F4-TCNQ. This indicates that whatever the starting alkyne, the charge transfers will only involve the cyanated parts and the aniline. This supposition is well supported by the TD-DFT calculations that showed that the central core played a very negligible role in the frontier orbitals and

thus in the electronic properties. The observed behavior is exclusively governed by the clicked moieties.

3. Conclusion

In conclusion, we have successfully applied the [2 + 2] CA-RE click reactions to a TPE platform adequately functionalized with electron-rich alkynes to obtain three cycloadducts, namely **TPE-TCNE**, **TPE-TCNQ** and **TPE-F_4-TCNQ.** All these cycloadducts were fully characterized by NMR spectroscopy and HR-MS spectrometry. As confirmed by ESR spectroscopy, **TPE-F_4-TCNQ** showed a substantial paramagnetic behavior in the solid state. As reported elsewhere, all compounds exhibited strong absorption bands in the NIR region of their UV-Visible absorption spectra, whose positions depend on the electron-withdrawing character of the clicked moieties. The origin of these bands were attributed by TD-DFT calculations to intramolecular charge transfers within the clicked moieties, indicating that the TPE core played a negligible role in the frontier orbitals and thus in the electronic properties. As a result, the **TPE-alkyne** precursor was rather luminescent with a QY of 21% and displayed a marked AIE behavior whereas among the clicked compounds, only **TPE-TCNE** showed a very faint fluorescence accompanied by an AIE behavior. Due to the fact that they are non-luminescent and that their CT band is in the NIR domain, **TPE-TCNQ** and **TPE-F_4-TCNQ** were found to be suitable candidates for photothermal studies. Upon irradiation with a laser beam at 808 nm, both compounds exhibited excellent photothermal properties; the best results being obtained with powders of **TPE-F_4-TCNQ**. In this case, a temperature of 100°C was reached within less than one minute without decomposition under a laser power of 2.58 W/cm². The present study shows that CA-RE click reactions provide an excellent strategy for conferring high performance photothermal properties to any molecular platform with appropriate functionalities and adequate thermal stability. This result is very interesting since it suggests that every already published or future CA-RE derivatives of TCNQ or F_4-TCNQ should be good candidates for photothermal applications.

Supplementary Materials: The following supporting information can be downloaded at the website of this paper posted on Preprints.org: synthetic procedures, materials and methods, additional NMR, IR and MS characterizations, UV-Visible absorption and fluorescence spectra, electrochemical data, photothermal and thermal analysis, TD-DFT calculations, Figures S1 to S47.

Author Contributions: Conceptualization, supervision and writing, S.C. and P.G.; synthesis, M.R., S.R.; electrochemistry and spectroelectrochemistry, Y.B., Y.T. and A.V.; TD-DFT calculations, I.A. and J.C.; photothermal measurements, G.F.; HR-MS characterizations, J.D.W.

Funding: This research was funded by the Ministère de l'Enseignement Supérieur, de la Recherche et de l'Innovation (MESRI) and by the Centre National de la Recherche Scientifique (CNRS).

Acknowledgments: P.G. and S.C. also thank Saad Séne for fruitful discussions and the staff of Plateau d'Analyse et de Caractérisation (PAC) of the Pole Balard of Montpellier for the spectral and thermal characterizations. The computational facilities in Mons are provided by the Consortium des Équipements de Calcul Intensif (CÉCI) funded by the Belgian National Fund for Scientific Research (F.R.S.-FNRS) for providing the computational resources. J.C. is an FNRS research director.

Conflicts of Interest: The authors declare no conflict of interest.

References

1. Braye, E.H.; Hübel, W.; Caplier, I. New Unsaturated Heterocyclic Systems. I. J. Am. Chem. Soc. 1961, 83, 4406-4413, doi:10.1021/ja01482a026.
2. Luo, J.; Xie, Z.; Lam, J.W.; Cheng, L.; Chen, H.; Qiu, C.; Kwok, H.S.; Zhan, X.; Liu, Y.; Zhu, D.; et al. Aggregation-induced emission of 1-methyl-1,2,3,4,5-pentaphenylsilole. Chem. Commun. 2001, 1740-1741.
3. Xia, Q.; Zhang, Y.; Li, Y.; Li, Y.; Li, Y.; Feng, Z.; Fan, X.; Qian, J.; Lin, H. A historical review of aggregation-induced emission from 2001 to 2020: A bibliometric analysis. Aggregate 2022, 3, e152, doi:10.1002/agt2.152.
4. Zhao, Z.; Zhang, H.; Lam, J.W.Y.; Tang, B.Z. Aggregation-Induced Emission: New Vistas at the Aggregate Level. Angew. Chem. Int. Ed. Engl. 2020, 59, 9888-9907, doi:10.1002/anie.201916729.

5. Zhang, H.; Liu, J.; Du, L.; Ma, C.; Leung, N.L.C.; Niu, Y.; Qin, A.; Sun, J.; Peng, Q.; Sung, H.H.Y.; et al. Drawing a clear mechanistic picture for the aggregation-induced emission process. Mater. Chem. Front., 2019, 3, 1143-1150, doi:10.1039/c9qm00156e.
6. Zhang, H.; Zhao, Z.; Turley, A.T.; Wang, L.; McGonigal, P.R.; Tu, Y.; Li, Y.; Wang, Z.; Kwok, R.T.K.; Lam, J.W.Y.; et al. Aggregate Science: From Structures to Properties. Adv. Mater. (Weinheim, Ger.) 2020, 32, 2001457, doi:10.1002/adma.202001457.
7. Xu, S.; Duan, Y.; Liu, B. Precise Molecular Design for High-Performance Luminogens with Aggregation-Induced Emission. Adv. Mater. 2020, 32, 1903530, doi:10.1002/adma.201903530.
8. Wan, Q.; Li, Y.; Ding, K.; Xie, Y.; Fan, J.; Tong, J.; Zeng, Z.; Li, Y.; Zhao, C.; Wang, Z.; et al. Aggregation Effect on Multiperformance Improvement in Aryl-Armed Phenazine-Based Emitters. J. Am. Chem. Soc. 2023, 145, 1607-1616, doi:10.1021/jacs.2c09210.
9. Jiang, W.; Zhang, G.; Zhao, G.; Wang, X.; Tian, W.; Sun, Y. Novel benzonitrile-based AIE host with high triplet energy for highly efficient solution-processed blue TADF OLEDs. Dyes Pigm. 2023, 210, 111037, doi:10.1016/j.dyepig.2022.111037.
10. Hwang, J.; Nagaraju, P.; Cho, M.J.; Choi, D.H. Aggregation-induced emission luminogens for organic light-emitting diodes with a single-component emitting layer. Aggregate 2023, 4, e199, doi:10.1002/agt2.199.
11. Amro, K.; Thakur, A.K.; Rolland, M.; Van Der Lee, A.; Lemaur, V.; Lazzaroni, R.; Rault-Berthelot, J.; Poriel, C.; Hirsch, L.; Clément, S.; et al. Linking triptycene to silole: a fruitful association. Mater. Chem. Front. 2020, 4, 2006-2017, doi:10.1039/D0QM00087F.
12. Anitha, O.; Mathivanan, M.; Tharmalingam, B.; Thiruppathiraja, T.; Ghorai, S.; Natarajan, R.; Thiagarajan, V.; Lakshmipathi, S.; Murugesapandian, B. Multi-stimuli responsiveness of pyrimidine bishydrazone: AIE, tuneable luminescence, white light emission, mechanochromism, acidochromism and its anticounterfeiting applications. Dyes Pigm. 2023, 212, 111091, doi:10.1016/j.dyepig.2023.111091.
13. Guo, X.; Song, T.; Chen, D.; Zhu, J.; Li, Z.; Xia, Q.; Wang, L.; Yang, W. Multi Stimuli-Responsive Aggregation-Induced Emission Active Polymer Platform Based on Tetraphenylethylene-Appended Maleic Anhydride Terpolymers. ACS Appl. Mater. Interfaces 2023, 15, 3543-3557, doi:10.1021/acsami.2c21668.
14. Deng, D.-d.; Zou, Y.; Chen, Z.; Liu, S.; Yang, Y.; Pu, S. Finely regulated benzothiadiazole derivatives: Aggregation-induced emission (AIE), hypso- or bathochromic mechanofluorochromic behaviors, and multilevel information encryption applications. Dyes Pigm. 2023, 211, 111051, doi:10.1016/j.dyepig.2022.111051.
15. Ahangar, A.A.; Ahmad, I.; Dar, A.A. AIE in the halogenated anils and their utilization as fluorescent probes for explosive nitro-aromatics. New J. Chem. 2023, 47, 4775-4783, doi:10.1039/d2nj05306c.
16. Amro, K.; Clément, S.; Déjardin, P.; Douglas, W.E.; Gerbier, P.; Janot, J.-M.; Thami, T. Supported thin flexible polymethylhydrosiloxane permeable films functionalised with silole groups: new approach for detection of nitroaromatics. J. Mater. Chem. 2010, 20, 7100-7103, doi:10.1039/C0JM01165G.
17. Zhang, Q.; Yin, B.; Hao, J.; Ma, L.; Huang, Y.; Shao, X.; Li, C.; Chu, Z.; Yi, C.; Wong, S.H.D.; et al. An AIEgen/graphene oxide nanocomposite (AIEgen@GO)-based two-stage "turn-on" nucleic acid biosensor for rapid detection of SARS-CoV-2 viral sequence. Aggregate 2023, 4, e195, doi:10.1002/agt2.195.
18. Xu, R.; Zhang, P.; Shen, Q.; Zhou, Y.; Wang, Z.; Xu, Y.; Meng, L.; Dang, D.; Ben, Z.T. AIE nanocrystals: Emerging nanolights with ultra-high brightness for biological application. Coord. Chem. Rev. 2023, 477, 214944, doi:10.1016/j.ccr.2022.214944.
19. Luo, W.; Tan, Y.; Gui, Y.; Yan, D.; Wang, D.; Tang, B.Z. Near-Infrared-Emissive AIE Bioconjugates: Recent Advances and Perspectives. Molecules 2022, 27, 3914, doi:10.3390/molecules27123914.
20. Wang, Z.; Zhou, Y.; Xu, R.; Xu, Y.; Dang, D.; Shen, Q.; Meng, L.; Tang, B.Z. Seeing the unseen: AIE luminogens for super-resolution imaging. Coord. Chem. Rev. 2022, 451, 214279, doi:10.1016/j.ccr.2021.214279.
21. Yan, D.; Qin, Y.; Yan, S.; Sun, P.; Wang, Y.; Wang, D.; Tang, B.Z. Near-infrared emissive AIE nanoparticles for biomedical applications: From the perspective of different nanocarriers. Particuology 2023, 74, 103-118, doi:10.1016/j.partic.2022.06.001.
22. Chua, M.H.; Chin, K.L.O.; Loh, X.J.; Zhu, Q.; Xu, J. Aggregation-Induced Emission-Active Nanostructures: Beyond Biomedical Applications. ACS Nano 2023, 17, 1845-1878, doi:10.1021/acsnano.2c10826.
23. Ingle, J.; Basu, S. Mitochondria Targeted AIE Probes for Cancer Phototherapy. ACS Omega 2023, 8, 8925-8935, doi:10.1021/acsomega.3c00203.

24. Yang, J.; Wang, Z.; Ge, J.; Deng, Y.; Ding, F.; Hu, L.; Wang, H. A deep-red emission AIE fluorescent probes based on coumarin for imaging lipid droplets in living cells. J. Mol. Struct. 2023, 1277, 134847, doi:10.1016/j.molstruc.2022.134847.
25. Ingle, J.; Sengupta, P.; Basu, S. Illuminating Sub-Cellular Organelles by Small Molecule AIEgens. ChemBioChem 2023, 24, e202200370, doi:10.1002/cbic.202200370.
26. Huang, X.; Zhang, S.; Liu, Z.; Cao, W.; Li, G.; Gao, W.; Tang, B. Novel AIE Probe for In Situ Imaging of Protein Sulfonation to Assess Cigarette Smoke-Induced Inflammatory Damage. Anal. Chem. 2023, 95, 1967-1974, doi:10.1021/acs.analchem.2c04267.
27. Kotras, C.; Fossepre, M.; Roger, M.; Gervais, V.; Richeter, S.; Gerbier, P.; Ulrich, S.; Surin, M.; Clement, S. A cationic tetraphenylethene as a light-up supramolecular probe for DNA G-quadruplexes. Front. Chem. 2019, 7, 493, doi:10.3389/fchem.2019.00493.
28. Arribat, M.; Remond, E.; Richeter, S.; Gerbier, P.; Clement, S.; Cavelier, F. Silole amino acids with aggregation-induced emission features synthesized by hydrosilylation. Eur. J. Org. Chem. 2019, 2019, 2275-2281, doi:10.1002/ejoc.201801869.
29. Pan, Z.; Wang, Y.; Chen, N.; Cao, G.; Zeng, Y.; Dong, J.; Liu, M.; Ye, Z.; Li, Y.; Huang, S.; et al. Aggregation-Induced emission photosensitizer with lysosomal response for photodynamic therapy against cancer. Bioorg. Chem. 2023, 132, 106349, doi:10.1016/j.bioorg.2023.106349.
30. Wang, X.; Xue, K.; Wang, X.; Zhao, Y.; Deng, J.; Yang, L.; Liang, J.; Li, Y.; Qi, Z. An aggregation-induced emission photosensitizer with efficient singlet oxygen generation capacity for mitochondria targeted photodynamic therapy. Dyes Pigm. 2023, 213, 111181.
31. Zhou, L.; Chen, L.; Chen, S.; Pu, Z.; Gu, M.; Shen, Y. Highly Efficient Photodynamic Therapy with Mitochondria-Targeting Aggregation-Induced Emission Photosensitizer for Retinoblastoma. Adv. Healthcare Mater. 2023, 12, 2202219, doi:10.1002/adhm.202202219.
32. Qu, R.; Zhen, X.; Jiang, X. Emerging designs of aggregation-induced emission agents for enhanced phototherapy applications. CCS Chem. 2022, 4, 401-419, doi:10.31635/ccschem.021.202101302.
33. Lin, Y.; Yi, M.; Guan, X.; Chen, E.; Yang, L.; Li, S.; Li, Y.; Zhang, L. "Two birds with one stone" strategy for the lung cancer therapy with bioinspired AIE aggregates. J. Nanobiotechnol. 2023, 21, 49, doi:10.1186/s12951-023-01799-1.
34. Jiang, W.; Cheng, C.; Qiu, X.; Chen, L.; Guo, X.; Luo, Y.; Wang, J.; Wang, J.; Xie, Z.; Li, P.; et al. Peptide Supramolecular Assembly-Instructed In Situ Self-Aggregation for Stratified Targeting Sonodynamic Therapy Enhancement of AIE Luminogens. Adv. Sci. 2023, 10, 2204989, doi:10.1002/advs.202204989.
35. Wu, M.-Y.; Chen, L.; Chen, Q.; Hu, R.; Xu, X.; Wang, Y.; Li, J.; Feng, S.; Dong, C.; Zhang, X.-L.; et al. Engineered Phage with Aggregation-Induced Emission Photosensitizer in Cocktail Therapy against Sepsis. Adv. Mater. 2023, 35, 2208578, doi:10.1002/adma.202208578.
36. Zhang, T.; Chen, X.; Yuan, C.; Pang, X.; Shangguan, P.; Liu, Y.; Han, L.; Sun, J.; Lam, J.W.Y.; Liu, Y.; et al. Near-Infrared Aggregation-Induced Emission Luminogens for In Vivo Theranostics of Alzheimer's Disease. Angew. Chem., Int. Ed. 2023, 62, e202211550, doi:10.1002/anie.202211550.
37. Liu, S.; Li, Y.; Kwok, R.T.K.; Lam, J.W.Y.; Tang, B.Z. Structural and process controls of AIEgens for NIR-II theranostics. Chem. Sci. 2020, 12, 3427-3436, doi:10.1039/d0sc02911d.
38. Liu, Y.; Li, Y.; Koo, S.; Sun, Y.; Liu, Y.; Liu, X.; Pan, Y.; Zhang, Z.; Du, M.; Lu, S.; et al. Versatile Types of Inorganic/Organic NIR-IIa/IIb Fluorophores: From Strategic Design toward Molecular Imaging and Theranostics. Chem. Rev. 2022, 122, 209-268, doi:10.1021/acs.chemrev.1c00553.
39. Xu, C.; Pu, K. Second near-infrared photothermal materials for combinational nanotheranostics. Chem. Soc. Rev. 2021, 50, 1111-1137, doi:10.1039/d0cs00664e.
40. Shao, A.; Xie, Y.; Zhu, S.; Guo, Z.; Zhu, S.; Guo, J.; Shi, P.; James, T.D.; Tian, H.; Zhu, W.H. Far-Red and Near-IR AIE-Active Fluorescent Organic Nanoprobes with Enhanced Tumor-Targeting Efficacy: Shape-Specific Effects. Angew. Chem. Int. Ed. Engl. 2015, 54, 7275-7280, doi:10.1002/anie.201501478.
41. Gu, X.; Yao, J.; Zhang, G.; Zhang, C.; Yan, Y.; Zhao, Y.; Zhang, D. New electron-donor/acceptor-substituted tetraphenylethylenes: aggregation-induced emission with tunable emission color and optical-waveguide behavior. Chem. Asian. J. 2013, 8, 2362-2369, doi:10.1002/asia.201300451.
42. Xu, W.; Lee, M.M.S.; Zhang, Z.; Sung, H.H.Y.; Williams, I.D.; Kwok, R.T.K.; Lam, J.W.Y.; Wang, D.; Tang, B.Z. Facile synthesis of AIEgens with wide color tunability for cellular imaging and therapy. Chem. Sci. 2019, 10, 3494-3501, doi:10.1039/c8sc05805a.

43. Ajayaghosh, A. Donor–acceptor type low band gap polymers: polysquaraines and related systems. Chem. Soc. Rev. 2003, 32, 181-191, doi:10.1039/B204251G.
44. Zhou, T.; Jia, T.; Kang, B.; Li, F.; Fahlman, M.; Wang, Y. Nitrile-substituted QA derivatives: new acceptor materials for solution-processable organic bulk heterojunction solar cells. Adv. Energy Mater. 2011, 1, 431-439, doi:10.1002/aenm.201100082.
45. Kolb, H.C.; Finn, M.G.; Sharpless, K.B. Click chemistry: diverse chemical function from a few good reactions. Angew. Chem., Int. Ed. 2001, 40, 2004-2021, doi:10.1002/1521-3773(20010601)40:11<2004::aid-anie2004>3.0.co;2-5.
46. Michinobu, T.; Diederich, F. The [2+2] Cycloaddition-Retroelectrocyclization (CA-RE) Click Reaction: Facile Access to Molecular and Polymeric Push-Pull Chromophores. Angew. Chem. Int. Ed. 2018, 57, 3552-3577, doi:10.1002/anie.201711605.
47. Shoji, T.; Ito, S. Azulene-based donor-acceptor systems: synthesis, optical, and electrochemical properties. Chem. - Eur. J. 2017, 23, 16696-16709, doi:10.1002/chem.201702806.
48. Bruce, M.I.; Rodgers, J.R.; Snow, M.R.; Swincer, A.G. Cyclopentadienyl-ruthenium and -osmium chemistry. Cleavage of tetracyanoethylene under mild conditions: X-ray crystal structures of [Ru{η3-C(CN)2CPhCC(CN)2}(PPh3)(η-C5H5)] and [Ru{C[C(CN)2]CPhC(CN)2}-(CNBut)(PPh3)(η-C5H5)]. J. C. S, Chem Comm. 1981, 6, 271-272.
49. Cai, C.; Liakatas, I.; Wong, M.-S.; Bösch, M.; Bosshard, C.; Günter, P.; Concilio, S.; Tirelli, N.; Suter, U.W. Donor−Acceptor-Substituted Phenylethenyl Bithiophenes: Highly Efficient and Stable Nonlinear Optical Chromophores. Org. Lett. 1999, 1, 1847-1849, doi:10.1021/ol991118r.
50. Wu, X.; Wu, J.; Liu, Y.; Jen, A.K.Y. Highly Efficient, Thermally and Chemically Stable Second Order Nonlinear Optical Chromophores Containing a 2-Phenyl-tetracyanobutadienyl Acceptor. J. Am. Chem. Soc. 1999, 121, 472-473, doi:10.1021/ja983537+.
51. Michinobu, T.; Boudon, C.; Gisselbrecht, J.P.; Seiler, P.; Frank, B.; Moonen, N.N.; Gross, M.; Diederich, F. Donor-substituted 1,1,4,4-tetracyanobutadienes (TCBDS): new chromophores with efficient intramolecular charge-transfer interactions by atom-economic synthesis. Chem. Eur. J 2006, 12, 1889-1905, doi:10.1002/chem.200501113.
52. Michinobu, T.; May, J.C.; Lim, J.H.; Boudon, C.; Gisselbrecht, J.-P.; Seiler, P.; Gross, M.; Biaggio, I.; Diederich, F. A new class of organic donor–acceptor molecules with large third-order optical nonlinearities. Chem. Commun. 2005, 737-739.
53. Kivala, M.; Boudon, C.; Gisselbrecht, J.P.; Enko, B.; Seiler, P.; Muller, I.B.; Langer, N.; Jarowski, P.D.; Gescheidt, G.; Diederich, F. Organic super-acceptors with efficient intramolecular charge-transfer interactions by [2+2] cycloadditions of TCNE, TCNQ, and F4-TCNQ to donor-substituted cyanoalkynes. Chem. Eur. J. 2009, 15, 4111-4123, doi:10.1002/chem.200802563.
54. Kivala, M.; Boudon, C.; Gisselbrecht, J.-P.; Seiler, P.; Gross, M.; Diederich, F. A novel reaction of 7,7,8,8-tetracyanoquinodimethane (TCNQ): charge-transfer chromophores by [2 + 2] cycloaddition with alkynes. Chem. Commun. 2007, 4731-4733, doi:10.1039/b713683h.
55. Reutenauer, P.; Kivala, M.; Jarowski, P.D.; Boudon, C.; Gisselbrecht, J.P.; Gross, M.; Diederich, F. New strong organic acceptors by cycloaddition of TCNE and TCNQ to donor-substituted cyanoalkynes. Chem. Commun. 2007, 4898-4900.
56. Patil, Y.; Misra, R. Diketopyrrolopyrrole-Based and Tetracyano-Bridged Small Molecules for Bulk Heterojunction Organic Solar Cells. Chem. - Asian J. 2018, 13, 220-229, doi:10.1002/asia.201701493.
57. Rout, Y.; Chauhan, V.; Misra, R. Synthesis and Characterization of Isoindigo-Based Push-Pull Chromophores. J. Org. Chem. 2020, 85, 4611-4618, doi:10.1021/acs.joc.9b03267.
58. Rao, P.S.; More, V.G.; Jangale, A.D.; Bhosale, S.V.; Bhosale, R.S.; Puyad, A.L.; Chen, J.-Y.; Li, J.-L.; Bhosale, S.V.; Gupta, A.; et al. A series of V-shaped small molecule non-fullerene electron acceptors for efficient bulk-heterojunction devices. Dyes Pigm. 2019, 171, 107677, doi:10.1016/j.dyepig.2019.107677.
59. Rao, P.S.; Puyad, A.L.; Bhosale, S.V.; Bhosale, S.V. Triphenylamine-merocyanine-based D1-A1-π-A2/A3-D2 chromophore system: synthesis, optoelectronic, and theoretical studies. Int. J. Mol. Sci. 2019, 20, 1621, doi:10.3390/ijms20071621.
60. Rout, Y.; Misra, R.; Singhal, R.; Biswas, S.; Sharma, G.D. Phenothiazine-based small-molecule organic solar cells with power conversion efficiency over 7% and open circuit voltage of about 1.0 V using solvent vapor annealing. Phys. Chem. Chem. Phys. 2018, 20, 6321-6329, doi:10.1039/c7cp08308d.

61. Srinivasa Rao, P.; Gupta, A.; Bhosale, S.V.; Bilic, A.; Xiang, W.; Evans, R.A.; Bhosale, S.V. Donor-acceptor-acceptor-based non-fullerene acceptors comprising terminal chromen-2-one functionality for efficient bulk-heterojunction devices. Dyes Pigm. 2017, 146, 502-511, doi:10.1016/j.dyepig.2017.07.047.
62. Gautam, P.; Misra, R.; Sharma, G.D. Dicyanoquinodimethane-substituted benzothiadiazole for efficient small-molecule solar cells. Phys. Chem. Chem. Phys. 2016, 18, 7235-7241, doi:10.1039/c6cp00243a.
63. He, W.; Washino, Y.; Murata, K.; Nozaki, N.; Matsumoto, H.; Michinobu, T. [2+2] Cycloaddition-retroelectrocyclization reactivity and thin film transistor performances of carbazole-based platinum polyyne polymers. Mater. Chem. Phys. 2022, 281, 125861, doi:10.1016/j.matchemphys.2022.125861.
64. Leliège, A.; Blanchard, P.; Rousseau, T.; Roncali, J. Triphenylamine/Tetracyanobutadiene-Based D-A-D π-Conjugated Systems as Molecular Donors for Organic Solar Cells. Org. Lett. 2011, 13, 3098-3101, doi:10.1021/ol201002j.
65. Raheem, A.A.; Murugan, P.; Shanmugam, R.; Praveen, C. Azulene Bridged π-Distorted Chromophores: The Influence of Structural Symmetry on Optoelectrochemical and Photovoltaic Parameters. ChemPlusChem 2021, 86, 1451-1460, doi:10.1002/cplu.202100392.
66. Philippe, C.; Melan, J.; Barsella, A.; Vives, T.; Leroux, Y.R.; Robin-Le Guen, F.; Lemiegre, L.; Jacquemin, D.; Gauthier, S.; Trolez, Y. A comprehensive study of tetracyanobutadiene push-pull chromophores derived from γ-pyranylidene. Tetrahedron Chem 2023, 5, doi:10.1016/j.tchem.2023.100036.
67. Pokladek, Z.; Ripoche, N.; Betou, M.; Trolez, Y.; Mongin, O.; Olesiak-Banska, J.; Matczyszyn, K.; Samoc, M.; Humphrey, M.G.; Blanchard-Desce, M.; et al. Linear Optical and Third-Order Nonlinear Optical Properties of Some Fluorenyl- and Triarylamine-Containing Tetracyanobutadiene Derivatives. Chem. Eur. J. 2016, 22, 10155-10167, doi:10.1002/chem.201600897.
68. Ripoche, N.; Betou, M.; Philippe, C.; Trolez, Y.; Mongin, O.; Dudek, M.; Pokladek, Z.; Matczyszyn, K.; Samoc, M.; Sahnoune, H.; et al. Two-photon absorption properties of multipolar triarylamino/tosylamido 1,1,4,4-tetracyanobutadienes. Phys. Chem. Chem. Phys. 2021, 23, 22283-22297, doi:10.1039/d1cp03346h.
69. Mammadova, F.; Inyurt, F.C.; Barsella, A.; Dengiz, C. Cyano-rich donor-acceptor-donor-type NLOphores containing dialkylated triazene and aniline groups. Dyes Pigm. 2023, 209, 110894, doi:10.1016/j.dyepig.2022.110894.
70. Zhao, P.; Wang, D.; Gao, H.; Zhang, J.; Xing, Y.; Yang, Z.; Cao, H.; He, W. Third-order nonlinear optical properties of the "clicked" closed-ring spiropyrans. Dyes Pigm. 2019, 162, 451-458, doi:10.1016/j.dyepig.2018.10.050.
71. Miao, Z.; Han, H.; Wang, D.; Gao, H.; Gu, J.; Hu, H. Nonlinear optical and energy-level modulation of organic alkynes by click chemistry. Tetrahedron 2016, 72, 4039-4046, doi:10.1016/j.tet.2016.05.035.
72. Yang, L.; Li, L.; Gao, H.; Wang, D.; Yang, Z.; Cao, H.; He, W. Photoacoustic effect of azo derivatives modified by click reagents and parceled by liposomes. Dyes Pigm. 2020, 172, 107822, doi:10.1016/j.dyepig.2019.107822.
73. Gao, H.; Zhao, Z.; Liu, W.; Wang, D.; He, W.; Cao, H.; Yang, Z. Novel application of NIR photoacoustic absorbing dyes in thermosensitive micelles. Dyes Pigm. 2019, 164, 319-326, doi:10.1016/j.dyepig.2019.01.053.
74. Zhao, Z.; Wang, D.; Gao, H.; Yang, Z.; Cao, H.; He, W. Photoacoustic effect of near-infrared absorbing fullerene derivatives with click moieties. Dyes Pigm. 2019, 164, 182-187, doi:10.1016/j.dyepig.2019.01.022.
75. Li, L.; Wang, D.; Wang, L.; Ramella, D.; Wang, H.; Gao, H.; Zhang, J.; Xing, Y.; Li, B.; Yang, Z.; et al. The photoacoustic effect of near-infrared absorbing porphyrin derivatives prepared via click chemistry. Dyes Pigm. 2018, 148, 501-507, doi:10.1016/j.dyepig.2017.08.003.
76. Xu, A.-P.; Han, H.-H.; Lu, J.; Yang, P.-P.; Gao, Y.-J.; An, H.-W.; Zhanng, D.; Li, L.-Z.; Zhang, J.-P.; Wang, D.; et al. Charge transfer NIR dyes for improved photoacoustic effect. Dyes Pigm. 2016, 125, 392-398, doi:10.1016/j.dyepig.2015.11.003.
77. Shi, H.; Gu, R.; Xu, W.; Huang, H.; Xue, L.; Wang, W.; Zhang, Y.; Si, W.; Dong, X. Near-Infrared Light-Harvesting Fullerene-Based Nanoparticles for Promoted Synergetic Tumor Phototheranostics. ACS Appl. Mater. Interfaces 2019, 11, 44970-44977, doi:10.1021/acsami.9b17716.
78. Tang, B.; Qin, A.; Han, P.; Zhang, G.; Xu, H. Preparation of organic near-infrared photothermal materials and its application. CN115043756, 2022.
79. Zhao, Z.; Lu, P.; Lam, J.W.Y.; Wang, Z.; Chan, C.Y.K.; Sung, H.H.Y.; Williams, I.D.; Ma, Y.; Tang, B.Z. Molecular anchors in the solid state: Restriction of intramolecular rotation boosts emission efficiency of luminogen aggregates to unity. Chem. Sci. 2011, 2, 672-675, doi:10.1039/c0sc00521e.

80. Philippe, C.; Coste, M.; Bretonniere, Y.; Lemiegre, L.; Ulrich, S.; Trolez, Y. Quadruple Functionalization of a Tetraphenylethylene Aromatic Scaffold with Ynamides or Tetracyanobutadienes: Synthesis and Optical Properties. Eur. J. Org. Chem. 2022, 2022, e202200049, doi:10.1002/ejoc.202200049.
81. Zhao, Z.; Chen, C.; Wu, W.; Wang, F.; Du, L.; Zhang, X.; Xiong, Y.; He, X.; Cai, Y.; Kwok, R.T.K.; et al. Highly efficient photothermal nanoagent achieved by harvesting energy via excited-state intramolecular motion within nanoparticles. Nat. Commun. 2019, 10, 768, doi:10.1038/s41467-019-08722-z.
82. Fesser, P.; Iacovita, C.; Wäckerlin, C.; Vijayaraghavan, S.; Ballav, N.; Howes, K.; Gisselbrecht, J.-P.; Crobu, M.; Boudon, C.; Stöhr, M.; et al. Visualizing the Product of a Formal Cycloaddition of 7,7,8,8-Tetracyano-p-quinodimethane (TCNQ) to an Acetylene-Appended Porphyrin by Scanning Tunneling Microscopy on Au(111). Chem. Eur. J. 2011, 17, 5246-5250, doi:10.1002/chem.201100733.
83. Liu, X.; Wang, D.; Gao, H.; Yang, Z.; Xing, Y.; Cao, H.; He, W.; Wang, H.; Gu, J.; Hu, H. Nonlinear optical properties of symmetrical and asymmetrical porphyrin derivatives with click chemistry modification. Dyes Pigm. 2016, 134, 155-163, doi:10.1016/j.dyepig.2016.07.010.
84. Wang, D.; Zhang, W.; Xing, Y.; Gao, H.; Wang, X.; Zhao, Y.; Yang, H. Energy-level modulation of organic alkynes by click chemistry. Tetrahedron 2013, 69, 895-901, doi:10.1016/j.tet.2012.10.081.
85. Zhao, Y.; Liu, X.; Li, Q.; Guo, Z.; He, Z.; Zhang, H.; Ma, C.; Gao, J.; Zhao, Y.; Wang, D. Preparation of Polyphenylene Ring Derivative Dyes with Wide Wave Absorption Properties and Their Performance Study. Molecules 2022, 27, 5551, doi:10.3390/molecules27175551.
86. Zhao, Y.; Liu, X.; Zhao, X.; Li, Q.; Zhao, Y.; Guo, Z.; He, Z.; Zhang, H.; Gao, J.; Miao, Z. Preparation of symmetrical and asymmetrical multi-phenylene ring nonlinear optical materials with click chemical modifications and their properties. Tetrahedron 2022, 127, 132992, doi:10.1016/j.tet.2022.132992.
87. Dar, A.H.; Gowri, V.; Gopal, A.; Muthukrishnan, A.; Bajaj, A.; Sartaliya, S.; Selim, A.; Ali, E.M.; Jayamurugan, G. Designing of Push-Pull Chromophores with Tunable Electronic and Luminescent Properties Using Urea as the Electron Donor. J. Org. Chem. 2019, 84, 8941-8947, doi:10.1021/acs.joc.9b00841.
88. Simon Marques, P.; Castan, J.M.A.; Raul, B.A.L.; Londi, G.; Ramirez, I.; Pshenichnikov, M.S.; Beljonne, D.; Walzer, K.; Blais, M.; Allain, M.; et al. Triphenylamine/Tetracyanobutadiene-Based π-Conjugated Push-Pull Molecules End-Capped with Arene Platforms: Synthesis, Photophysics, and Photovoltaic Response. Chem. - Eur. J. 2020, 26, 16422-16433, doi:10.1002/chem.202002810.
89. Philippe, C.; Bui, A.T.; Beau, M.; Bloux, H.; Riobe, F.; Mongin, O.; Roisnel, T.; Cordier, M.; Paul, F.; Lemiegre, L.; et al. Synthesis and Photophysical Properties of 1,1,4,4-Tetracyanobutadienes Derived from Ynamides Bearing Fluorophores. Chem. - Eur. J. 2022, 28, e202200025, doi:10.1002/chem.202200025.
90. Parr, R.G.; Yang, W. Density-functional Theory of Atoms and Molecules; Clarendon Press: 1989.
91. Runge, E.; Gross, E.K.U. Density-functional theory for time-dependent systems. Phys. Rev. Lett. 1984, 52, 997-1000, doi:10.1103/physrevlett.52.997.
92. Stratmann, R.E.; Scuseria, G.E.; Frisch, M.J. An efficient implementation of time-dependent density-functional theory for the calculation of excitation energies of large molecules. J. Chem. Phys. 1998, 109, 8218-8224, doi:10.1063/1.477483.
93. Trickey, S.B. Recent Advances in Density Functional Methods -Part I by Delano P. Chong. Int. J. Quantum Chem. 1999, 72, 155-156.
94. Zhao, Y.; Truhlar, D.G. Density Functionals with Broad Applicability in Chemistry. Acc. Chem. Res. 2008, 41, 157-167, doi:10.1021/ar700111a.
95. Yanai, T.; Tew, D.P.; Handy, N.C. A new hybrid exchange-correlation functional using the Coulomb-attenuating method (CAM-B3LYP). Chem. Phys. Lett. 2004, 393, 51-57, doi:10.1016/j.cplett.2004.06.011.
96. Adamo, C.; Jacquemin, D. The calculations of excited-state properties with Time-Dependent Density Functional Theory. Chem. Soc. Rev. 2013, 42, 845-856, doi:10.1039/c2cs35394f.
97. Martin, R.L. Natural transition orbitals. J. Chem. Phys. 2003, 118, 4775-4777, doi:10.1063/1.1558471.
98. Etienne, T.; Assfeld, X.; Monari, A. Toward a Quantitative Assessment of Electronic Transitions' Charge-Transfer Character. J. Chem. Theory Comput. 2014, 10, 3896-3905, doi:10.1021/ct5003994.
99. Etienne, T.; Assfeld, X.; Monari, A. New Insight into the Topology of Excited States through Detachment/Attachment Density Matrices-Based Centroids of Charge. J. Chem. Theory Comput. 2014, 10, 3906-3914, doi:10.1021/ct500400s.
100. Han, P.; Zhang, G.; Xu, H.; Hu, R.; Qin, A.; Tang, B.Z. Organic near infrared photothermal materials with temperatures up to 450°C constructed by cycloaddition-retroelectrocyclization click reaction. ChemRxiv 2022, 1-32.

101. Banziger, S.D.; Clendening, R.A.; Oxley, B.M.; Ren, T. Spectroelectrochemical and Computational Analysis of a Series of Cycloaddition-Retroelectrocyclization-Derived Donor-Acceptor Chromophores. J. Phys. Chem. B 2020, 124, 11901-11909, doi:10.1021/acs.jpcb.0c09450.
102. Gautam, P.; Maragani, R.; Misra, R. Tuning the HOMO-LUMO gap of donor-substituted benzothiazoles. Tetrahedron Lett. 2014, 55, 6827-6830, doi:10.1016/j.tetlet.2014.10.094.
103. Jin, Z.; Wang, D.; Wang, X.; Liang, P.; Mi, Y.; Yang, H. Efficient modification of pyrene-derivative featuring third-order nonlinear optics via the click post-functionalization. Tetrahedron Lett. 2013, 54, 4859-4864, doi:10.1016/j.tetlet.2013.06.121.
104. Liang, P.; Du, Z.; Wang, D.; Yang, Z.; Sheng, H.; Liang, S.; Cao, H.; He, W.; Yang, H. Optoelectronic and Self-assembly Properties of Porphyrin Derivatives with Click Chemistry Modification. ChemPhysChem 2014, 15, 3523-3529, doi:10.1002/cphc.201402401.
105. Mi, Y.; Liang, P.; Jin, Z.; Wang, D.; Yang, Z. Synthesis and Third-Order Nonlinear Optical Properties of Triphenylene Derivatives Modified by Click Chemistry. ChemPhysChem 2013, 14, 4102-4108, doi:10.1002/cphc.201300615.
106. Misra, R.; Gautam, P. Tuning of the HOMO-LUMO gap of donor-substituted symmetrical and unsymmetrical benzothiadiazoles. Org. Biomol. Chem. 2014, 12, 5448-5457, doi:10.1039/c4ob00629a.
107. Rout, Y.; Gautam, P.; Misra, R. Unsymmetrical and Symmetrical Push-Pull Phenothiazines. J. Org. Chem. 2017, 82, 6840-6845, doi:10.1021/acs.joc.7b00991.
108. Rout, Y.; Jang, Y.; Gobeze, H.B.; Misra, R.; D'Souza, F. Conversion of Large-Bandgap Triphenylamine-Benzothiadiazole to Low-Bandgap, Wide-Band Capturing Donor-Acceptor Systems by Tetracyanobutadiene and/or Dicyanoquinodimethane Insertion for Ultrafast Charge Separation. J. Phys. Chem. C 2019, 123, 23382-23389, doi:10.1021/acs.jpcc.9b06632.
109. Sharma, R.; Maragani, R.; Misra, R. C3-Symmetric star shaped donor-acceptor truxenes: synthesis and photophysical, electrochemical and computational studies. New J. Chem. 2018, 42, 882-890, doi:10.1039/c7nj03934d.
110. Sharma, R.; Thomas, M.B.; Misra, R.; D'Souza, F. Strong Ground- and Excited-State Charge Transfer in C3-Symmetric Truxene-Derived Phenothiazine-Tetracyanobutadine and Expanded Conjugates. Angew. Chem., Int. Ed. 2019, 58, 4350-4355, doi:10.1002/anie.201814388.
111. Zhang, W.-S.; Wang, D.; Cao, H.; Yang, H. Energy level tunable pre-click functionalization of [60]fullerene for nonlinear optics. Tetrahedron 2014, 70, 573-577, doi:10.1016/j.tet.2013.12.018.
112. Zhang, Z.; Gou, G.; Wan, J.; Li, H.; Wang, M.; Li, L. Synthesis, Structure, and Significant Energy Gap Modulation of Symmetrical Silafluorene-Cored Tetracyanobutadiene and Tetracyanoquinodimethane Derivatives. J. Org. Chem., doi:10.1021/acs.joc.1c02382.